

RESEARCH ARTICLE

Coherent feedback leads to robust background compensation in oscillatory and non-oscillatory homeostats

Melissa Nygård, Peter Ruoff *

Department of Chemistry, Bioscience, and Environmental Engineering, University of Stavanger, Stavanger, Norway

* peter.ruoff@uis.no

OPEN ACCESS

Citation: Nygård M, Ruoff P (2023) Coherent feedback leads to robust background compensation in oscillatory and non-oscillatory homeostats. PLoS ONE 18(8): e0287083. <https://doi.org/10.1371/journal.pone.0287083>

Editor: Karthik Raman, Indian Institute of Technology Madras, INDIA

Received: May 29, 2023

Accepted: August 14, 2023

Published: August 28, 2023

Peer Review History: PLOS recognizes the benefits of transparency in the peer review process; therefore, we enable the publication of all of the content of peer review and author responses alongside final, published articles. The editorial history of this article is available here: <https://doi.org/10.1371/journal.pone.0287083>

Copyright: © 2023 Nygård, Ruoff. This is an open access article distributed under the terms of the [Creative Commons Attribution License](https://creativecommons.org/licenses/by/4.0/), which permits unrestricted use, distribution, and reproduction in any medium, provided the original author and source are credited.

Data Availability Statement: All relevant data are within the paper and its [Supporting information files](#).

Funding: The author(s) received no specific funding for this work.

Abstract

When in a reaction kinetic integral controller a step perturbation is applied besides a constant background, the concentration of a controlled variable (described as A) will generally respond with decreased response amplitudes ΔA as backgrounds increase. The controller variable E will at the same time provide the necessary compensatory flux to move A back to its set-point. A typical example of decreased response amplitudes at increased backgrounds is found in retinal light adaptation. Due to remarks in the literature that retinal light adaptation would also involve a compensation of backgrounds we became interested in conditions how background compensation could occur. In this paper we describe novel findings how background influences can be robustly eliminated. When such a background compensation is active, oscillatory controllers will respond to a defined perturbation with always the same (damped or undamped) frequency profile, or in the non-oscillatory case, with the same response amplitude ΔA , irrespective of the background level. To achieve background compensation we found that two conditions need to apply: (i) an additional set of integral controllers (here described as I_1 and I_2) have to be employed to keep the manipulated variable E at a defined set-point, and (ii), I_1 and I_2 need to feed back to the A - E signaling axis directly through the controlled variable A . In analogy to a similar feedback applied in quantum control theory, we term these feedback conditions as ‘coherent feedback’. When analyzing retinal light adaptations in more detail, we find no evidence of the presence of background compensation mechanisms. Although robust background compensation, as described theoretically here, appears to be an interesting regulatory property, relevant biological or biochemical examples still need to be identified.

Introduction

Homeostatic mechanisms play important roles in physiology and in the adaptation of organisms to their environments [1]. For example, vertebrate retinal photoreceptor cells contain negative feedback loops which participate in light adaptation [2–5]. A hallmark of vertebrate photoadaptation is that resetting kinetics accelerate and response amplitudes decrease as backgrounds increase [5, 6]. This behavior is seen in [Fig 1](#) for a macaque monkey’s rod cell response towards a single light flash applied at different background light levels.

Competing interests: The authors have declared that no competing interests exist.

Another retinal light adaptation example is shown in Fig 2. Here, the mean maximum firing rates of a cat ganglion cell was measured with respect to different step light perturbations (test spot luminance) which are applied at six different backgrounds [8].

Kandel et al. [2] commented (see page 540, section *Light Adaptation Is Apparent in Retinal Processing and Visual Perception*) that Fig 2 would indicate a compensation of the background illumination and thereby causing the same response due to a lateral shifting along the perturbation (test spot luminance) axis. Based on this comment we became interested in mechanisms which would allow to compensate for background levels and thereby give the same response for a given perturbation irrespective of the applied background. In this paper we present results on how such a robust background compensation can be achieved in both oscillatory and non-oscillatory homeostats.

The paper is structured in the following way: We first show that a feedback type similar to what quantum physicists have termed ‘coherent feedback’ [9, 10] is required to obtain background compensation in both oscillatory and non-oscillatory homeostats. For oscillatory homeostats we show that coherent feedback control leads to background compensation and to frequency control. Although we previously observed robust frequency control [11], we did not recognize at that time the background-compensating property of coherent feedback. For non-

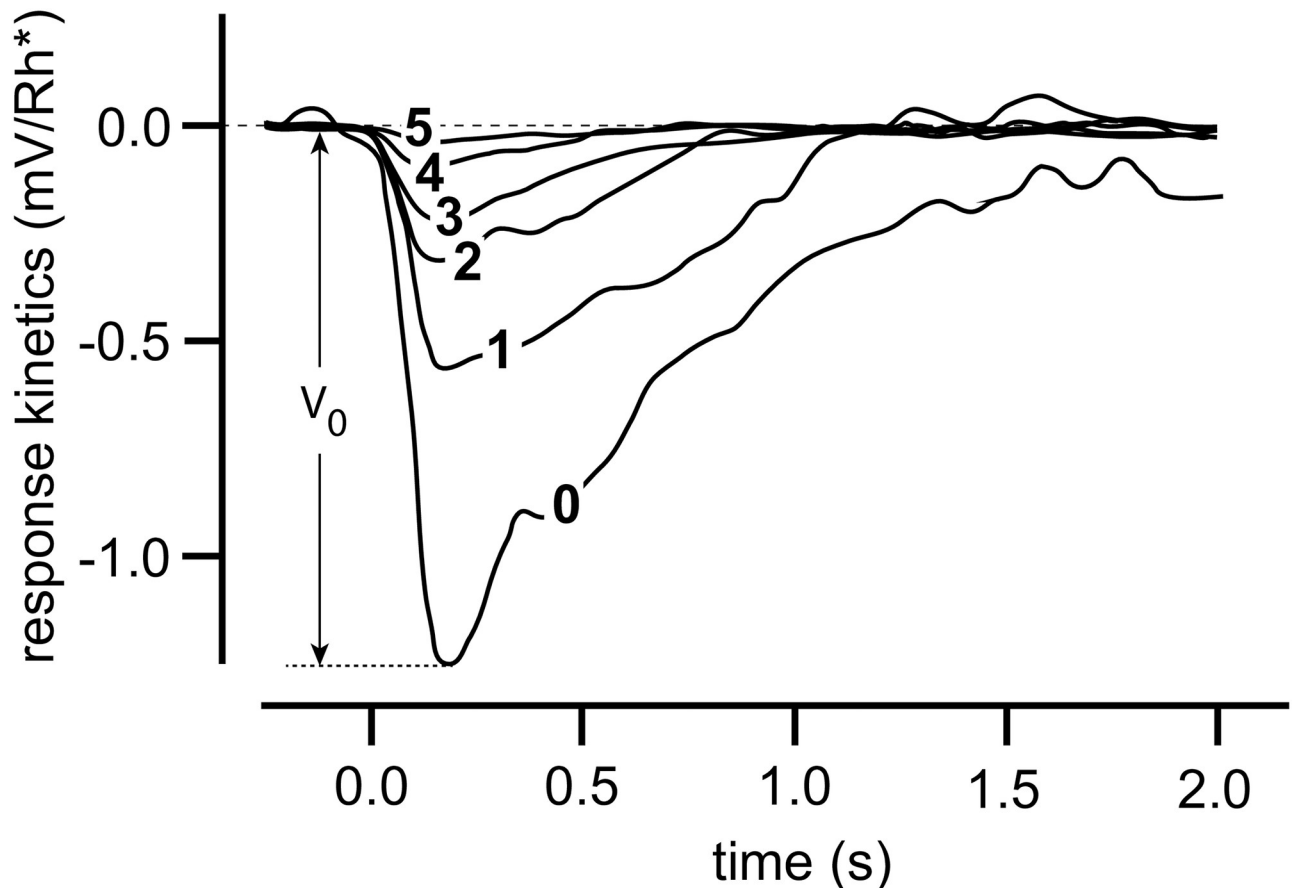


Fig 1. Light adaptation in a macaque monkey's rod cell. 10 ms light flashes were applied to different light background intensities. Background intensities (in photons $\mu\text{m}^{-2}\text{s}^{-1}$) were: 0, 0; 1, 3.1; 2, 12; 3, 41; 4, 84; 5, 162. The influence of the background on the response amplitude and the speed of resetting is clearly seen. V_0 is the response amplitude for background 0. Redrawn and modified after Fig 2A from Ref [7]. For a theoretical description of this behavior see Ref [5] and references therein.

<https://doi.org/10.1371/journal.pone.0287083.g001>

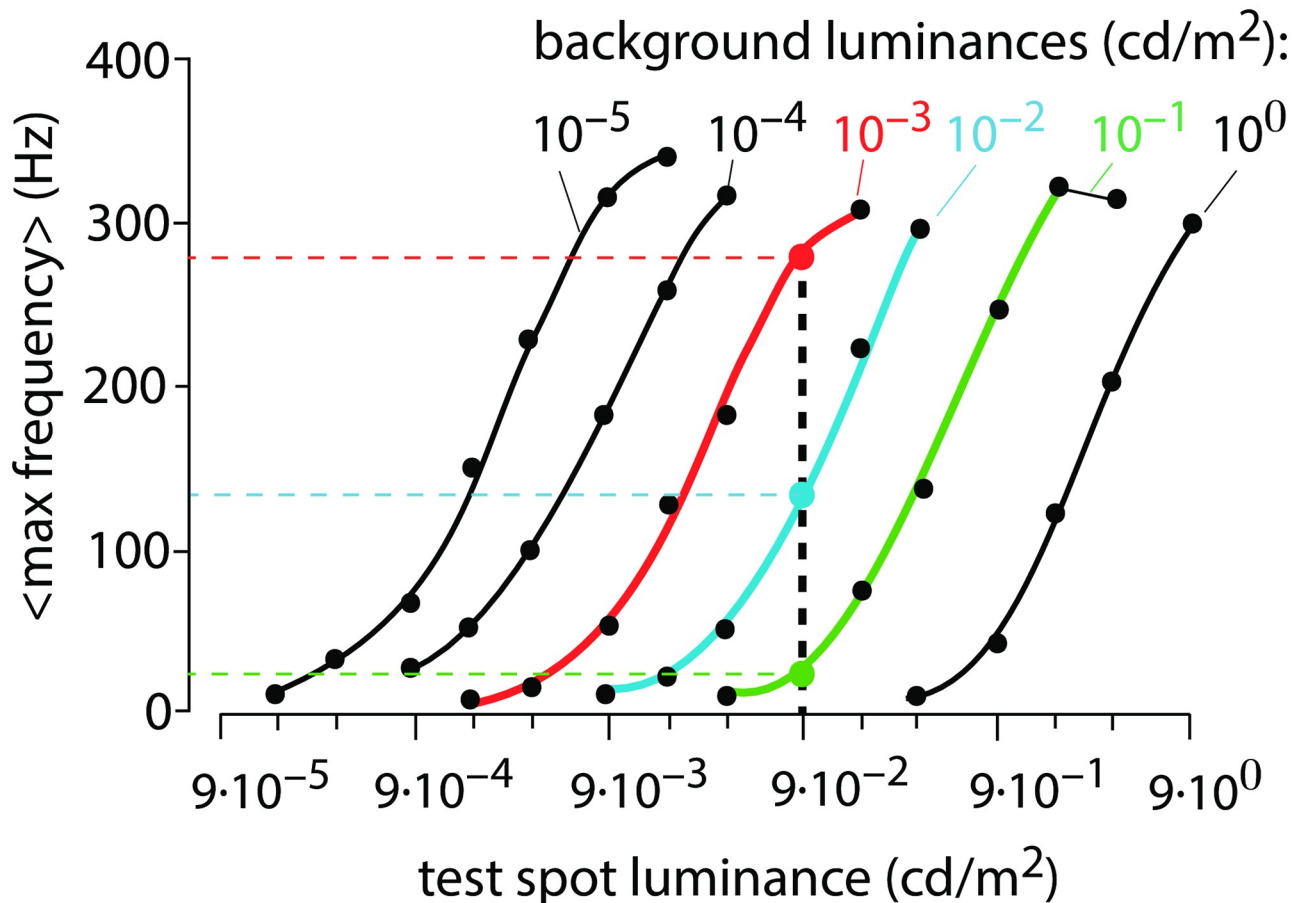


Fig 2. Light adaptation of an on-center ganglion cell in the cat retina (redrawn from Fig 8, Ref [8]). Averaged maximum ganglion cell frequencies are shown as a function of six different background illuminations in response to applied light step perturbations (test spot luminance). The three colored curves show the averaged maximum frequencies at background illuminations 10^{-3} , 10^{-2} and 10^{-1} cd/m^2 . A test spot luminance (perturbation) of 9×10^{-2} cd/m^2 is indicated as the vertical dashed black line. The colored intersection points and vertical dashed lines indicate that for this perturbation strength the maximum mean response frequency decreases with increasing background illumination.

<https://doi.org/10.1371/journal.pone.0287083.g002>

oscillatory controllers or homeostats with damped oscillations, coherent feedback leads to conserved response profiles in the controlled variables, independent of an applied background. We then look at the situation of a ‘incoherent feedback’, where background compensation is lost, but oscillatory homeostats may still show robust frequency control. Finally, we analyze photoreceptor responses in terms of a model based on the Hill equation, as described by Dowling [3]. We show that parallel lines as in Fig 2, or as log-log plots, do not require the postulation of background compensation or additional adaptation mechanisms.

Materials and methods

Computations were performed with the Fortran subroutine LSODE [12], which can be downloaded from <https://computing.llnl.gov/projects/odepack>. Graphical output was generated with gnuplot (www.gnuplot.info) and annotated with Adobe Illustrator (<https://www.adobe.com/>).

To make notations simpler, concentrations of compounds are denoted by compound names without square brackets. Time derivatives are generally indicated by the ‘dot’ notation.

Rate parameters are in arbitrary units (au) and are presented as k_i 's ($i = 1, 2, 3, \dots$) irrespective of their kinetic nature, i.e. whether they represent turnover numbers, Michaelis constants, or inhibition/activation constants. To allow readers to redo calculations, the supporting information [S1 Data](#) contains python scripts for a set of selected results.

Integral control, step perturbations and the background concept

In the calculations robust homeostasis of concentrations and frequencies is achieved by implementing integral control into the negative feedbacks, a concept which has its origin from control engineering [13–16], and has been indicated to occur also in biological systems [17–21]. Briefly, in integral control the difference (also termed error) between the actual concentration of a controlled variable A and its set-point is integrated in time. The integrated error can then be used to compensate precisely for stepwise perturbations [15, 16]. [Fig 3a](#) shows the control scheme of integral control. A reaction kinetic example is given in panel b using ‘motif 2’, which is one of eight basic negative feedback structures [22]. Note that the removal reactions of A have been divided into two parts: a perturbative removal by a stepwise change of k_1 (indicated in dark-red), and a constitutive removal of A , termed ‘background’, with a constant k_2 (indicated in dark-blue).

For example, when studying photoreceptor cells often a constant background light is used in addition to the application of a flash or step of light [2–4]. In fact, motif 2 has been found [5] to describe light adaptations and the influence of different background light intensities, as shown in [Fig 1](#), relatively well. In this paper we describe novel findings how a background can be compensated for, such that the response kinetics become independent of different but constant backgrounds.

There are several kinetic requirements which can lead to integral control. [Fig 3c](#) shows how a zero-order removal of controller species E results in integral control with a defined set-point A_{set} of the controlled variable A .

In the following calculations we have used zero-order kinetics to implement integral control [17, 22–24]. However, it should be mentioned that there are other kinetics conditions to achieve integral control, such as antithetic control [21, 25, 26], which often will show identical resetting behaviors as in zero-order control [5, 26]. Also, autocatalytic reactions can be used to obtain integral control [27–29], which generally will show much faster resetting kinetics in comparison when integral control is introduced by zero-order kinetics [30, 31].

Recently, mathematical methods has been put forward based on either linear [32, 33] or nonlinear [34] generic models to describe and analyze physiological control systems. These more mathematically inclined methods differ from the approach taken here, which is based on mass action kinetics.

Results and discussion

Background compensation in negative feedback oscillators by coherent feedback

In this section we describe feedback conditions which can achieve background compensation in oscillatory homeostats. The here considered oscillators show frequency homeostasis based on a two-layered negative feedback structure. A center integral feedback layer ensures that the time average of a controlled variable A , defined by [Eq 1](#), is kept robustly at set-point A_{set} by a

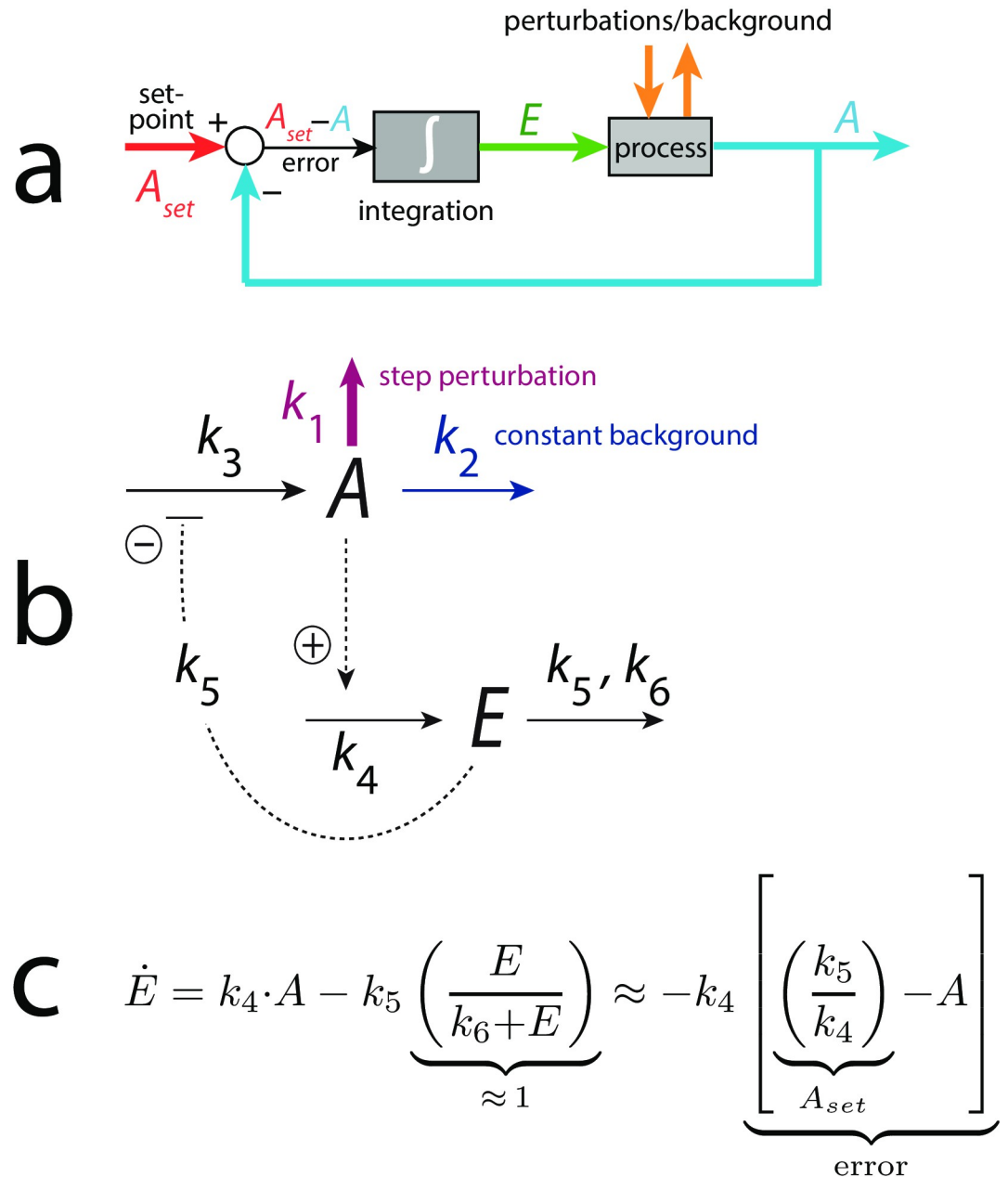


Fig 3. Integral control and the definition of background. Panel a: Principle of integral control. The controlled variable A (outlined in blue) is compared with its set-point and the difference/error ($A_{set} - A$) is integrated. This leads to the integrated error E , which is able to compensate precisely for stepwise perturbations [15]. Panel b: Basic negative feedback loop (motif 2, [22]). Solid lines are chemical reactions, while dashed lines represent activations (plus sign) and inhibitions (negative sign). The removal of A is divided into two parts, a perturbative part where k_1 can change stepwise (outlined in dark-red) and a background part where k_2 is kept constant (outlined in dark-blue). Panel c: Rate equation of controller E . The zero-order removal of E introduces integral control. The set-point for A (A_{set}) is given as k_5/k_4 , and the concentration of E becomes proportional to the integrated error [22]. For other ways to implement integral control, see text.

<https://doi.org/10.1371/journal.pone.0287083.g003>

controller species E .

$$\langle A \rangle (t) = \frac{1}{t} \int_0^t A(t') \cdot dt' \tag{1}$$

A second ‘outer’ negative feedback layer keeps on its side the time average value of E , i.e. $\langle E \rangle$ (Eq 2), under robust homeostatic control by two additional controller variables I_1 and I_2 .

$$\langle E \rangle (t) = \frac{1}{t} \int_0^t E(t') \cdot dt' \tag{2}$$

We previously showed [11] that such two-layered negative feedback structures enable robust frequency homeostasis. Here we report the additional and novel finding that when the I_1 and I_2 controllers feed back directly via A to control E , the oscillator has the capability to neutralize backgrounds. In analogy to a closely related feedback definition employed in quantum control theory and optics, we call this type of feedback for ‘coherent feedback’ (see [9, 10] and references therein).

Background compensation in a motif 2 based oscillatory homeostat. Fig 4a shows an example of a frequency-compensated oscillator which can compensate for different but constant backgrounds.

The center oscillator in Fig 4a is given by the A - e - E - A feedback loop based on derepression motif 2 [22], where E keeps $\langle A \rangle$ under homeostatic control (see rate equations and definitions of set-points below). Oscillations are promoted, because the removals of A and E are zero-order with respect to A and E , and thereby construct a quasi-conservative oscillator [11]. The intermediate e has been included to obtain limit-cycle oscillations [11]. I_1 and I_2 are controller species, which keep $\langle E \rangle$ under homeostatic control. It is the control of $\langle E \rangle$ by I_1 and I_2 , which allows for the frequency homeostasis of the oscillator [11]. Their A -coherent feedback directly to A allows for robust background compensation. Since the central A - e - E - A negative feedback is an inflow controller it principally can only compensate for outflow perturbations [22]. The considered outflow perturbations of A split into two components: a

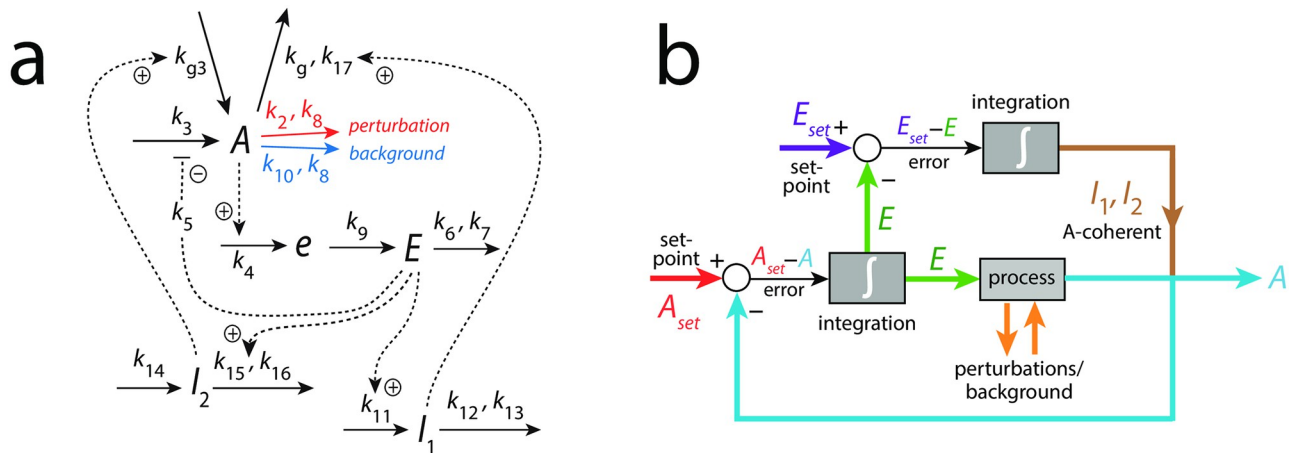


Fig 4. Frequency-compensated oscillator with background compensation by coherent feedback. Panel a: Reaction kinetic scheme based on derepression motif 2 (m2) [22] in the inner A - e - E - A negative feedback. Figs S12-S14 in the supporting information of Ref [11] describe some properties of this oscillator, but without having recognized at that time the ability to robustly compensate for backgrounds. Solid arrows indicate chemical reactions, while dashed lines show activations (plus signs) and one inhibition (minus sign). The addition of compound e was found [11] to promote limit-cycle oscillations. Panel b: Flow scheme indicating the additional control of E via A by controllers I_1 and I_2 .

<https://doi.org/10.1371/journal.pone.0287083.g004>

constant (zero-order) background with rate constant k_{10} (Fig 4a outlined in blue) and a (zero-order) perturbation part where rate constant k_2 undergoes a stepwise change (in Fig 4a outlined in red). Zero-order kinetics with respect to A are achieved by small k_8 and k_{17} values, i.e. $A/(k_8 + A) \approx 1$ and $A/(k_{17} + A) \approx 1$. Fig 4b shows the flow scheme and the control of E by I_1 and I_2 via the A -coherent part of the controller.

The rate equations are:

$$\dot{A} = k_{g3} \cdot I_2 + \frac{k_3 \cdot k_5}{k_5 + E} - \frac{k_8 \cdot A \cdot I_1}{k_{17} + A} - \underbrace{\frac{k_2 \cdot A}{k_8 + A}}_{\text{perturbation}} - \underbrace{\frac{k_{10} \cdot A}{k_8 + A}}_{\text{background}} \tag{3}$$

$$\dot{e} = k_4 \cdot A - k_9 \cdot e \tag{4}$$

$$\dot{E} = k_9 \cdot e - \frac{k_6 \cdot E}{k_7 + E} \tag{5}$$

$$\dot{I}_1 = k_{11} \cdot E - \frac{k_{12} \cdot I_1}{k_{13} + I_1} \tag{6}$$

$$\dot{I}_2 = k_{14} - \left(\frac{k_{15} \cdot I_2}{k_{16} + I_2} \right) \cdot E \tag{7}$$

The set-point of $\langle A \rangle$ (A_{set}) by controller E can be calculated from the steady state condition of the time averages:

$$k_4 \cdot \langle A_{ss} \rangle = k_9 \cdot \langle e_{ss} \rangle = k_6 \cdot \underbrace{\left(\frac{E_{ss}}{k_7 + E_{ss}} \right)}_{\approx 1 \text{ (zero-order)}} \Rightarrow \langle A_{ss} \rangle = A_{set} = \frac{k_6}{k_4} \tag{8}$$

In Eq 8 the zero-order condition with respect to E ensures a robust perfect adaptation of $\langle A_{ss} \rangle$ to A_{set} when the system oscillates, or a perfect adaptation of A to A_{set} in case the feedback loop is non-oscillatory [11]. Since the control of A by E is an inflow controller based on the derepression flux $k_3 \cdot k_5 / (k_5 + E)$, the controller is active whenever $\langle A \rangle$ is below A_{set} .

Variable E is controlled by I_1 and I_2 . They act as respectively outflow or inflow controllers [22] with respect to $\langle E \rangle$ (if oscillatory) or E (if non-oscillatory). Also here zero-order removals of both I_1 and I_2 ensure robust set-points. For controller I_1 the steady state condition gives:

$$k_{11} \cdot \langle E_{ss} \rangle = k_{12} \cdot \underbrace{\left(\frac{I_{1,ss}}{k_{13} + I_{1,ss}} \right)}_{\approx 1 \text{ (zero-order)}} \Rightarrow \langle E_{ss} \rangle = E_{set}^{I_1} = \frac{k_{12}}{k_{11}} \tag{9}$$

The I_1 outflow controller becomes active whenever $\langle E \rangle$ is higher than $E_{set}^{I_1}$.

The set-point for the I_2 inflow controller is determined by the steady state condition:

$$k_{14} = k_{15} \cdot \underbrace{\langle E_{ss} \rangle}_{\approx 1 \text{ (zero-order)}} \left(\frac{I_{2,ss}}{k_{16} + I_{2,ss}} \right) \Rightarrow \langle E_{ss} \rangle = E_{set}^{I_2} = \frac{k_{14}}{k_{15}} \quad (10)$$

The I_2 controller becomes active whenever $\langle E \rangle$ is lower than $E_{set}^{I_2}$. It should be noted that the values of the inflow/outflow set-points $E_{set}^{I_1}$ and $E_{set}^{I_2}$ need to follow certain rules to guarantee that inflow and outflow controllers cooperate. In this case $E_{set}^{I_2}$ should be lower than $E_{set}^{I_1}$, otherwise I_1 and I_2 will work against each other and windup will occur. For a discussion about windup in combined controllers, see Ref [22].

In the following we describe how the above oscillator behaves in presence of a stepwise perturbation at different but constant backgrounds. Fig 5 shows the oscillator's behavior for a stepwise perturbation in k_2 from 1.0 (phase 1) to 10.0 (phase 2) at a background $k_{10} = 0.0$. The time of change in k_2 is indicated in each panel by a vertical arrow. Panel a shows the oscillations in A together with its average $\langle A \rangle$ (Eq 1), while panel b shows E and $\langle E \rangle$ (Eq 2). Panel c shows the changes in I_1 and I_2 , and panel d shows the frequency (i.e. the inverse of the period length). The resetting of the frequency to its pre-perturbation value is clearly seen. If I_1 and I_2 would not be present, $\langle A \rangle$ would be kept at $A_{set} = 2.0$ by a reduced (derepressed) E as seen in

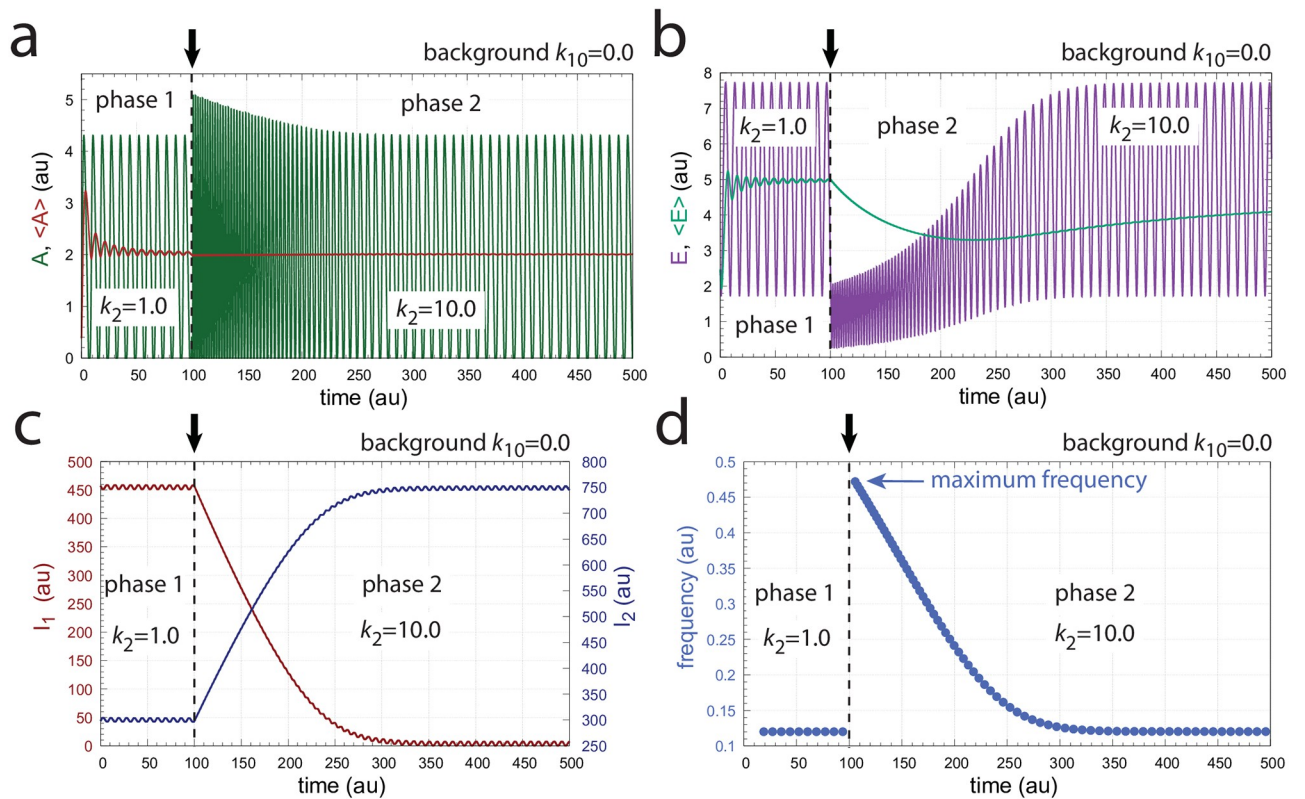


Fig 5. Frequency compensation in the feedback scheme of Fig 4a for a stepwise k_2 change (1.0 \rightarrow 10.0) at background $k_{10} = 0.0$. Vertical arrows indicate where the change in k_2 occurs. Other rate constants: $k_3 = 100.0$, $k_4 = 1.0$, $k_5 = 0.1$, $k_6 = 2.0$, $k_7 = k_8 = k_{13} = k_{16} = k_{17} = 1 \times 10^{-6}$, $k_9 = 20.0$, $k_{11} = 1.0$, $k_{12} = 5.0$, $k_{14} = 4.99$, $k_{15} = 1.0$, and $k_g = k_{g3} = 1 \times 10^{-2}$. Initial concentrations: $A_0 = 0.3780$, $E_0 = 2.4784$, $e_0 = 1.5993 \times 10^{-2}$, $I_{1,0} = 4.5727 \times 10^2$, $I_{2,0} = 2.9817 \times 10^2$ (see S1 Data for python script).

<https://doi.org/10.1371/journal.pone.0287083.g005>

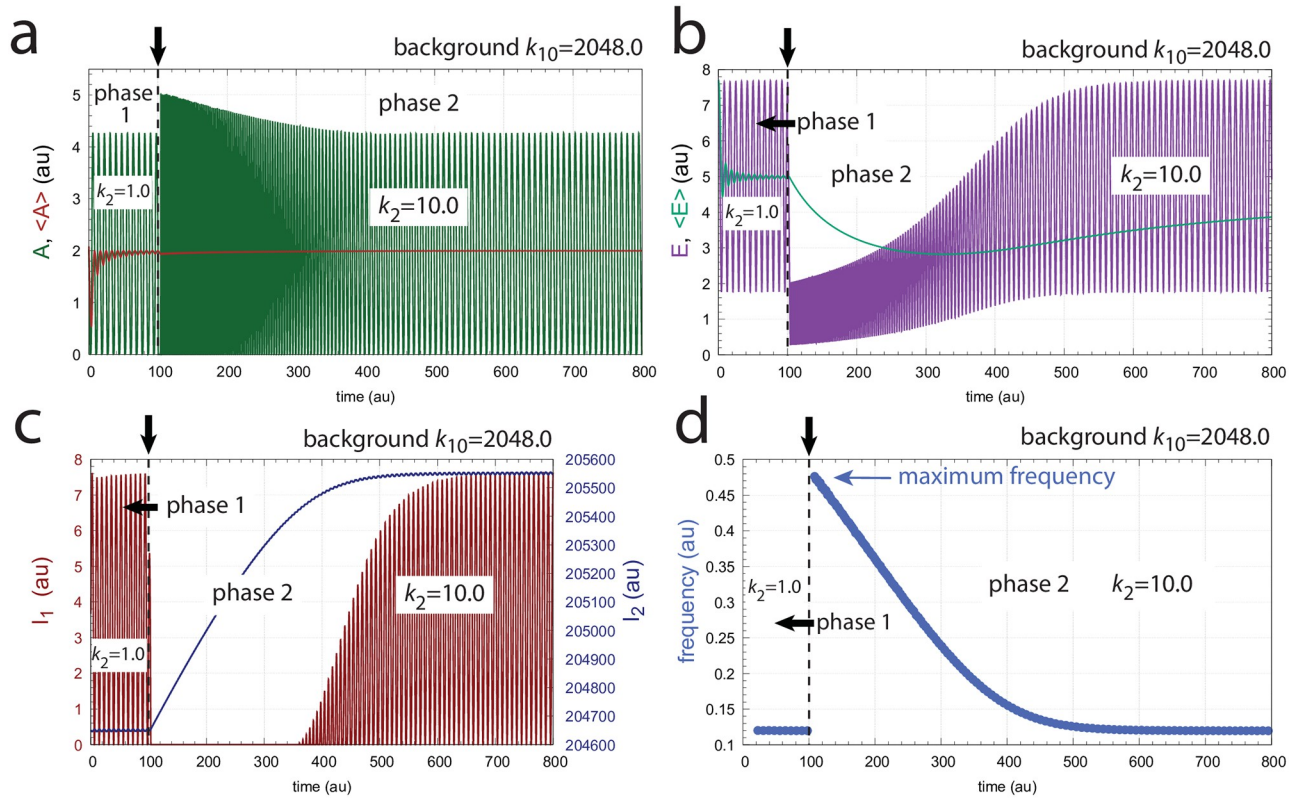


Fig 6. Frequency compensation in the feedback scheme of Fig 4a for a stepwise change in k_2 at background $k_{10} = 2048.0$. Vertical arrows indicate where the change in k_2 occurs. Other rate constants as in Fig 5. Initial concentrations: $A_0 = 2.1377, E_0 = 7.6720, e_0 = 1.0996 \times 10^{-1}, I_{1,0} = 3.4304, I_{2,0} = 2.0465 \times 10^5$ (see S1 Data for python script).

<https://doi.org/10.1371/journal.pone.0287083.g006>

panel b at 100 time units. However, since $\langle E \rangle$ is also controlled by I_1 and I_2 , i.e. between $5.0 (E_{set}^1 = 5.0)$ and $4.99 (E_{set}^2 = 4.99)$, I_1 and I_2 take over the control of both $\langle A \rangle$ and $\langle E \rangle$.

Fig 6 shows the same perturbation in k_2 as in Fig 5, but with a background of $k_{10} = 2048.0$. The increased removal of A by the background is compensated by an increase of I_2 and a decrease of I_1 , which keep $\langle A \rangle$ and $\langle E \rangle$ at their respective set-points. The maximum frequency, which occurs directly after the k_2 step is not affected by the changed background.

Fig 7 shows how the maximum frequency depends on k_2 steps at different but constant backgrounds k_{10} . The parallel lines which occur due to the unchanged maximum frequencies for a given background are indicative of “background compensation”.

Background compensation in a motif 8 (m8) based oscillatory homeostat. To provide an additional example of a frequency-compensated negative feedback oscillator with background compensation we use a m8 outflow control motif [22] for the center feedback loop. The scheme of this oscillator is shown in Fig 8. In this motif, the controlled variable A inhibits the generation of the controller E . Controller E on its side inhibits the removal of A . The outer controllers, I_1 and I_2 , feed directly back to A . As for the m2 controller, oscillations in the central m8 oscillator are facilitated by removing A and E by zero-order processes. The rate equations are (‘pert’ stands for perturbation and ‘bg’ for background):

$$\dot{A} = \underbrace{k_1}_{\text{pert}} + \underbrace{k_3}_{\text{bg}} - \left(\frac{k_{g2} \cdot A}{k_{18} + A} \right) \cdot I_2 + k_{g1} \cdot I_1 - \left(\frac{k_4 \cdot A}{k_5 + A} \right) \cdot \left(\frac{k_9}{k_9 + E} \right) \quad (11)$$

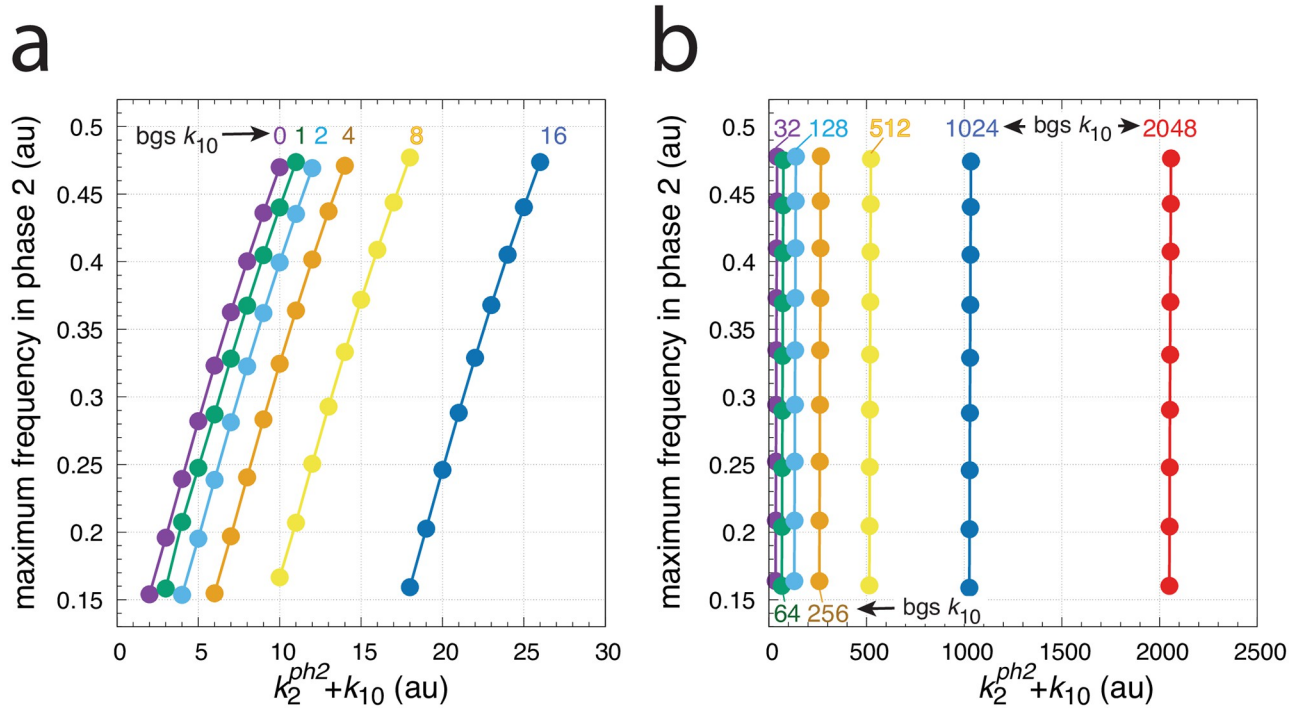


Fig 7. Background frequency compensation in the oscillator of Fig 4. The maximum frequency (see Figs 5d or 6d) is plotted as a function of $k_2^{ph2} + k_{10}$, where k_2^{ph2} is the k_2 value during phase 2. The maximum frequency is determined for different stepwise k_2 changes, i.e. for 1.0→2.0, 1.0→3.0, ..., 1.0→9.0, up to 1.0→10.0. The steps occur at time $t = 100$ at different but constant k_{10} backgrounds (bgs). Calculations have been performed analogous to Figs 5 and 6. The k_{10} background values are 0, 1, 2, 4, up to 2048 (indicated in the figure). Other rate constants as in Fig 5. Initial concentrations: bgs 0–128, as in Fig 5; bg 256, $A_0 = 0.9866$, $E_0 = 7.3508$, $e_0 = 5.2447 \times 10^{-2}$, $I_{1,0} = 5.8243$, $I_{2,0} = 2.5447 \times 10^4$; bg 512, $A_0 = 8.3872 \times 10^{-4}$, $E_0 = 4.8793$, $e_0 = 3.9572 \times 10^{-5}$, $I_{1,0} = 7.6544$, $I_{2,0} = 5.1046 \times 10^4$; bg 1024, $A_0 = 1.7657$, $E_0 = 7.6866$, $e_0 = 9.1430 \times 10^{-2}$, $I_{1,0} = 4.2379$, $I_{2,0} = 1.0225 \times 10^5$; bg 2048, as in Fig 6.

<https://doi.org/10.1371/journal.pone.0287083.g007>

$$\dot{e} = \frac{k_6 \cdot k_{10}}{k_{10} + A} - k_{11} \cdot e \tag{12}$$

$$\dot{E} = k_{11} \cdot e - \frac{k_7 \cdot E}{k_8 + E} \tag{13}$$

$$\dot{I}_1 = k_{12} \cdot E - \frac{k_{13} \cdot I_1}{k_{14} + I_1} \tag{14}$$

$$\dot{I}_2 = k_{15} - \left(\frac{k_{16} \cdot I_2}{k_{17} + I_2} \right) \cdot E \tag{15}$$

The inflow to A is divided into a stepwise perturbative component k_1 (indicated in Eq 11 by ‘pert’ and outlined in red in Fig 8) and a background k_3 (indicated in Eq 11 by ‘bg’ and outlined in blue in Fig 8). All other in- and outflows to and from A are compensatory fluxes.

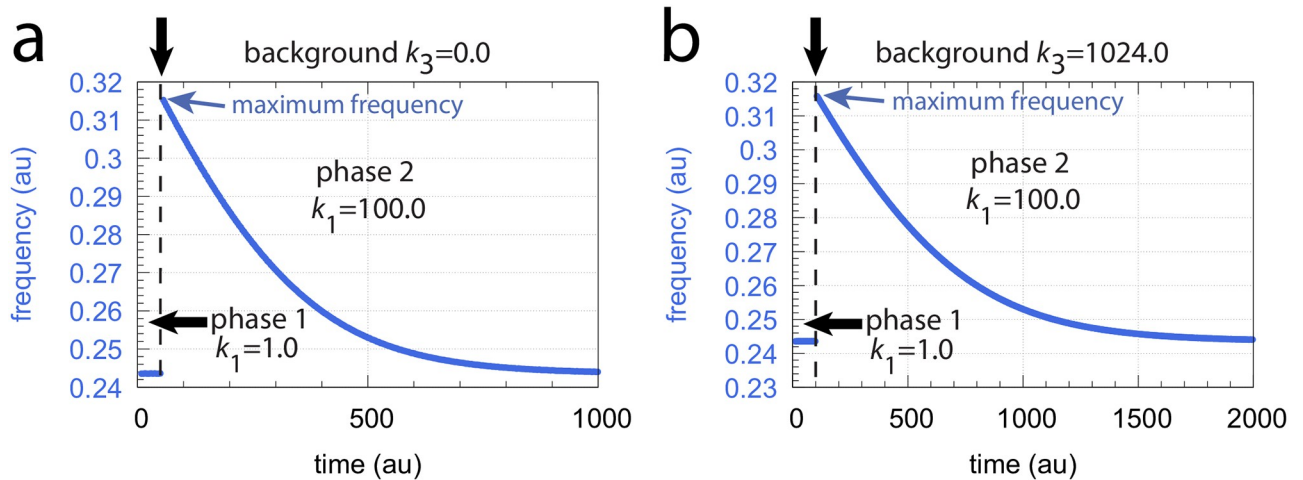


Fig 9. Frequency homeostasis in the oscillator described in Fig 8. In both panels a stepwise perturbation in k_1 from 1.0 (phase 1) to 100.0 (phase 2) is applied (the step is indicated by the vertical arrows on top of the plots). In panel a, a constant background of $k_3 = 0.0$ is applied (at both phases 1 and 2), while in panel b the background is 1024.0. Other rate constant values are: $k_4 = 1 \times 10^4$, $k_5 = k_8 = k_{14} = k_{17} = k_{18} = 1 \times 10^{-6}$, $k_6 = 1 \times 10^3$, $k_7 = 50.0$, $k_9 = 0.1$, $k_{11} = 1.0$, $k_{12} = 5.0$, $k_{13} = 50.00$, $k_{15} = 50.0$, $k_{16} = 1.0$ and $k_{g1} = k_{g2} = 1 \times 10^{-2}$. Initial concentrations ($k_3 = 0.0$): $A_0 = 3.3568 \times 10^2$, $E_0 = 2.6209 \times 10^1$, $e_0 = 7.3942$, $I_{1,0} = 2.4840 \times 10^4$, $I_{2,0} = 1.2768 \times 10^4$. Initial concentrations ($k_3 = 1024.0$): $A_0 = 3.6188$, $E_0 = 1.8696 \times 10^1$, $e_0 = 1.7115 \times 10^2$, $I_{1,0} = 4.6869$, $I_{2,0} = 9.0420 \times 10^4$. Two python scripts, which in addition show the variations of A , E , I_1 , and I_2 , are included in [S1 Data](#).

<https://doi.org/10.1371/journal.pone.0287083.g009>

Fig 9 shows that the oscillator described in Fig 8 shows frequency homeostasis at different but constant k_3 backgrounds. In panel a the background is $k_3 = 0.0$, while in panel b we have $k_3 = 1024.0$. In both cases the maximum frequency for a k_1 step of $1.0 \rightarrow 100.0$ is unchanged, indicating that the maximum frequency is background compensated.

Fig 10 shows the maximum frequencies for different k_1 steps and k_3 backgrounds. There, different but constant k_3 backgrounds are applied with values 0, 2, 4, 8, 16, 32, 64, 128, 256, 512, and 1024. Variable k_1 step perturbations are applied by starting with a 1.0 (phase 1) to 10.0 (phase 2) step and ending with a 1.0 (phase 1) to 500.0 (phase 2) step by successively increasing the k_1 values in phase 2 by 10.0. The figure shows that the maximum frequencies, although dependent on the k_1 step, remain unchanged with respect to an applied background k_3 . This behavior results in parallel lines when maximum frequencies are plotted against $k_1^{ph2} + k_3$.

Background compensation in non-oscillatory homeostats. In this section we look at background compensation in non-oscillatory homeostats where E is controlled by I_1 and I_2 via coherent feedback. We show two examples: in the first one the controller’s response after a step perturbation is significantly damped, while in the other example the response shows a larger train of (damped) oscillations. In both cases the response profiles of the controlled variables A and E are preserved and independent of the background.

For the first example we use the oscillator scheme from Fig 4a. To go over to a non-oscillatory mode, we change the kinetics for all A -removing reactions from zero-order to first-order kinetics with respect to A . The rate equation of A becomes (compare with Eq 3):

$$\dot{A} = k_1 + k_{g3} \cdot I_2 + \frac{k_3 \cdot k_5}{k_5 + E} - k_g \cdot A \cdot I_1 - \underbrace{k_2 \cdot A}_{\text{perturbation}} - \underbrace{k_{10} \cdot A}_{\text{background}} \tag{18}$$

while the rate equations for the other components (Eqs 4–7) remain the same.

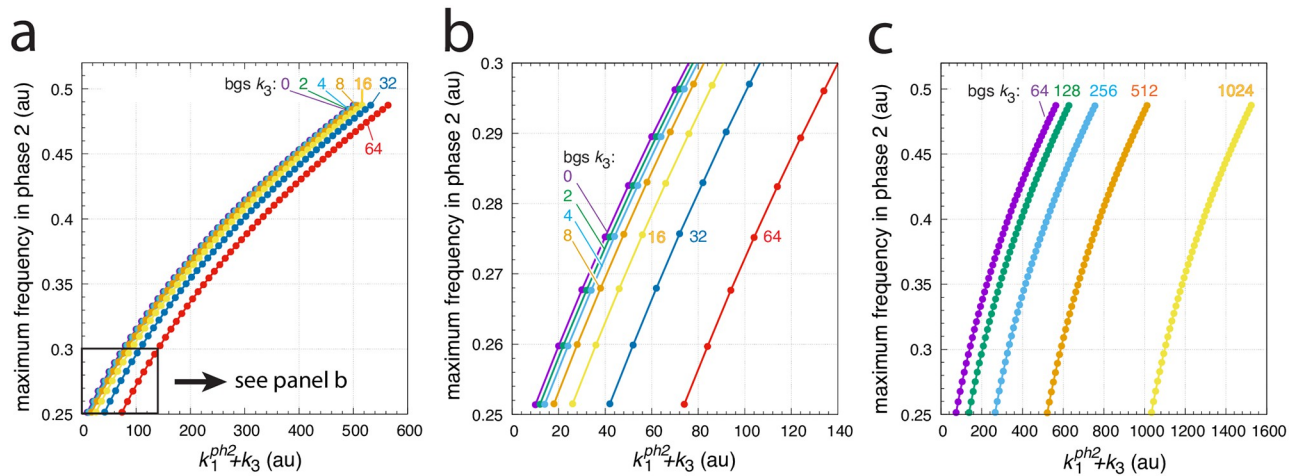


Fig 10. Background (bg) frequency compensation in the oscillator of Fig 8. The maximum frequency (see Fig 9) is plotted as a function of the sum of k_1^{ph2} and background k_3 , where k_1 is the k_1 value in phase 2. In analogy with the calculations in Figs 5 and 6, the maximum frequency is determined for different stepwise k_1 changes, i.e. for 1.0→10.0, 1.0→20.0, . . . , 1.0→30.0, up to 1.0→500.0, which occur at time $t = 100$ at different but constant k_3 backgrounds (bgs). The k_3 background values are 0, 2, 4, up to 1024 (indicated in the figure). Other rate constants as described in Fig 9. Initial concentrations: bg 0: as in Fig 9a; bg 2: $A_0 = 3.4008 \times 10^2$, $E_0 = 2.3906 \times 10^1$, $e_0 = 7.0224$, $I_{1,0} = 2.4739 \times 10^4$, $I_{2,0} = 1.2869 \times 10^4$; bg 4: $A_0 = 3.4461 \times 10^2$, $E_0 = 2.1393 \times 10^1$, $e_0 = 6.6417$, $I_{1,0} = 2.4637 \times 10^4$, $I_{2,0} = 1.2971 \times 10^4$; bg 8: $A_0 = 4.8073 \times 10^2$, $E_0 = 6.0165 \times 10^1$, $e_0 = 1.0914 \times 10^2$, $I_{1,0} = 2.4401 \times 10^4$, $I_{2,0} = 1.3207 \times 10^4$; bg 16: $A_0 = 4.3570$, $E_0 = 1.9953 \times 10^1$, $e_0 = 1.6964 \times 10^2$, $I_{1,0} = 2.4005 \times 10^4$, $I_{2,0} = 1.3603 \times 10^4$; bg 32: $A_0 = 3.9151 \times 10^1$, $E_0 = 5.4663 \times 10^1$, $e_0 = 1.1875 \times 10^2$, $I_{1,0} = 2.3201 \times 10^4$, $I_{2,0} = 1.4407 \times 10^4$; bg 64: $A_0 = 3.0270 \times 10^2$, $E_0 = 4.1000 \times 10^1$, $e_0 = 1.0456 \times 10^1$, $I_{1,0} = 2.1646 \times 10^4$, $I_{2,0} = 1.5962 \times 10^4$; bg 128: $A_0 = 3.2021 \times 10^2$, $E_0 = 3.3534 \times 10^1$, $e_0 = 8.7470$, $I_{1,0} = 1.8443 \times 10^4$, $I_{2,0} = 1.9165 \times 10^4$; bg 256: $A_0 = 6.4511 \times 10^1$, $E_0 = 6.8158 \times 10^1$, $e_0 = 9.3623 \times 10^1$, $I_{1,0} = 1.2002 \times 10^4$, $I_{2,0} = 2.5606 \times 10^4$; bg 512: $A_0 = 2.6297 \times 10^2$, $E_0 = 5.5584 \times 10^1$, $e_0 = 1.5294 \times 10^1$, $I_{1,0} = 3.2525 \times 10^3$, $I_{2,0} = 4.2375 \times 10^4$; bg 1024: as in Fig 9b. Panel a shows an overview of the maximum frequencies up to background 64, while panel b shows a blown-up part indicated in panel a. Panel c shows the maximum frequencies for backgrounds in the range between 64 to 1024.

<https://doi.org/10.1371/journal.pone.0287083.g010>

Fig 11 gives an overview of the results. In panel a the maximum excursions ΔA after the step (see inset) are plotted for different backgrounds k_{10} as a function of the sum of the phase 2 k_2 value and k_{10} . For each background, the nine k_2 steps 1→2, 1→3, . . . , 1→9, and 1→10 are applied and ΔA is determined. For a certain defined k_2 -step ΔA is independent of the background (k_{10}), which leads to the parallel lines in panel a. Panel b shows the situation for a k_2 1→10 step when background $k_{10} = 0$. In panel c the same step is applied, but the background has been increased to $k_{10} = 10$. Comparing Fig 11b and 11c shows that profiles in both A and E are the same with $A_{set} = 2.0$ and $E_{set} = 100$.

Fig 13 shows another example of coherent feedback. Here we have two inflow controllers E_1 and E_2 , but only E_2 is connected to A via I_1 and I_2 through a coherent feedback. The reason why we looked at two E -controllers was to see whether E_2 alone, i.e. without the help of I_1 and I_2 , was able to compensate backgrounds. This, however, turned out not to be the case and I_1 and I_2 were included to control E_2 .

The rate equations are:

$$\dot{A} = k_g \cdot I_2 - k_{g3} \cdot A \cdot I_1 - k_2 \cdot A - k_{10} \cdot A + k_9 \cdot a + k_{11} \cdot E_2 \tag{19}$$

$$\dot{a} = \frac{k_3 \cdot k_5}{k_5 + E_1} - k_9 \cdot a \tag{20}$$

$$\dot{E}_1 = k_4 \cdot A - \frac{k_6 \cdot E_1}{k_7 + E_1} \tag{21}$$

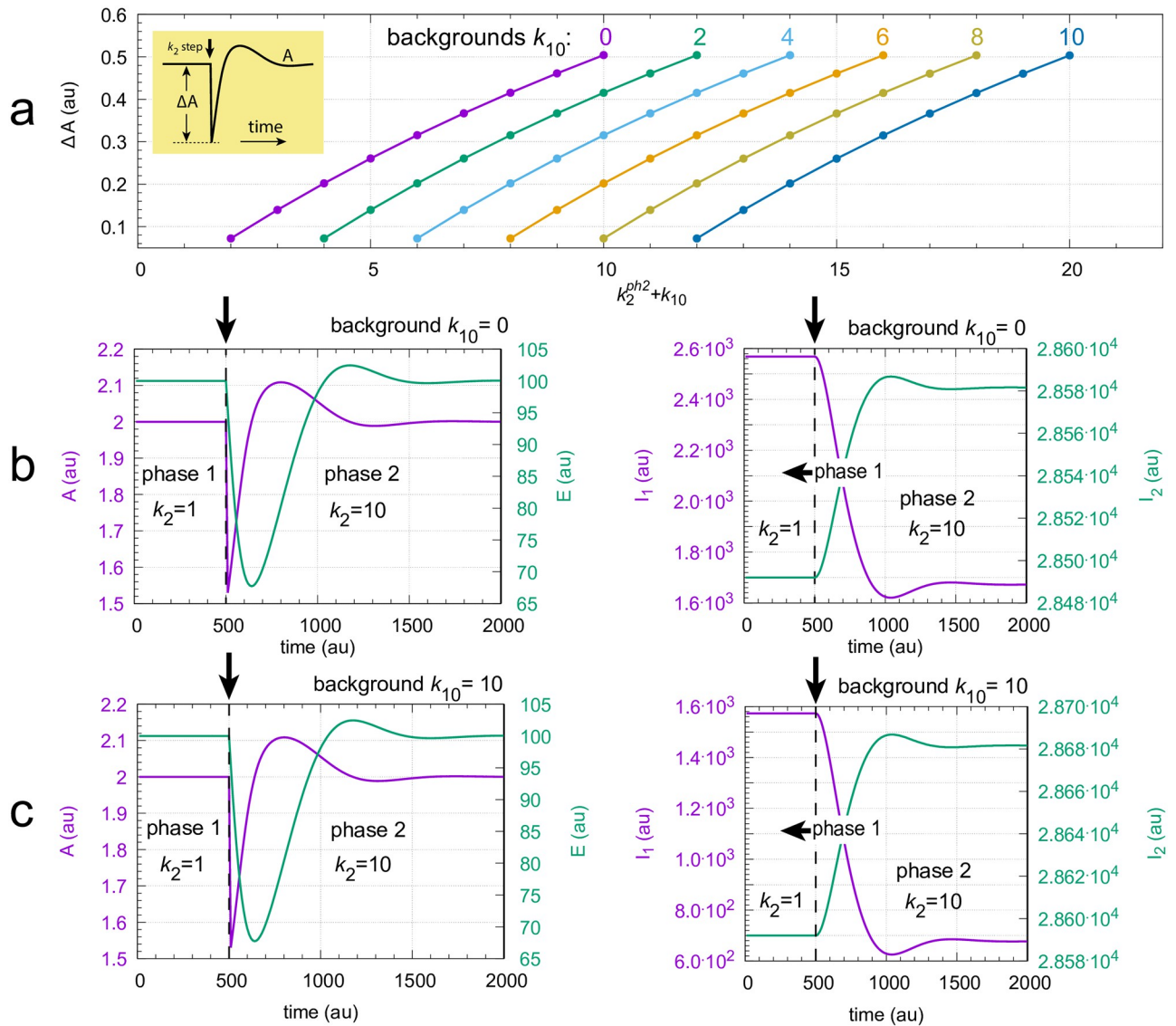


Fig 11. Background compensation in the non-oscillatory feedback scheme of Fig 12. Panel a: Each colored curve shows the values of ΔA for the nine k_2 steps: $1 \rightarrow 2, 1 \rightarrow 3, \dots, 1 \rightarrow 10$ at k_{10} background levels: $0, 2, 4, \dots, 8, 10$. Inset shows how ΔA is defined. k_2^{ph2} is the value of k_2 during phase 2. Panels in b: Time profiles of A, E (left panel) and I_1, I_2 (right panel) for a $1 \rightarrow 10$ k_2 step at background $k_{10} = 0.0$. The change in k_2 is applied at time $t = 500$, which is indicated by the vertical arrows. Panels in c are similar to the panels in b with the difference that background k_{10} is 10.0 . Other rate constants: $k_3 = 5 \times 10^3, k_4 = 1.0, k_5 = 0.5, k_6 = 2.0, k_7 = 1 \times 10^{-5}, k_8 = 2.0, k_9 = 2.0, k_{11} = 0.1, k_{12} = 10.0, k_{13} = k_{16} = 1 \times 10^{-4}, k_{14} = 1.0, k_{15} = 0.01, k_g = 0.01, k_{g^3} = 1 \times 10^{-3}$. Initial concentrations for panel b: $A_0 = 2.0, E_0 = 100.0, e_0 = 1.0, I_{1,0} = 2.5684 \times 10^3, I_{2,0} = 2.8492 \times 10^4$. Initial concentrations for panel c: $A_0 = 2.0, E_0 = 100.0, e_0 = 1.0, I_{1,0} = 1.5734 \times 10^3, I_{2,0} = 2.8592 \times 10^4$. For python scripts showing the results of panels b and c, please see supporting information [S1 Data](#).

<https://doi.org/10.1371/journal.pone.0287083.g011>

$$\dot{E}_2 = k_{12} - A \cdot \left(\frac{k_{13} \cdot E_2}{k_{14} + E_2} \right) \tag{22}$$

$$\dot{I}_1 = k_{15} - \left(\frac{k_{16} \cdot I_1}{k_{17} + I_1} \right) \cdot E_2 \tag{23}$$

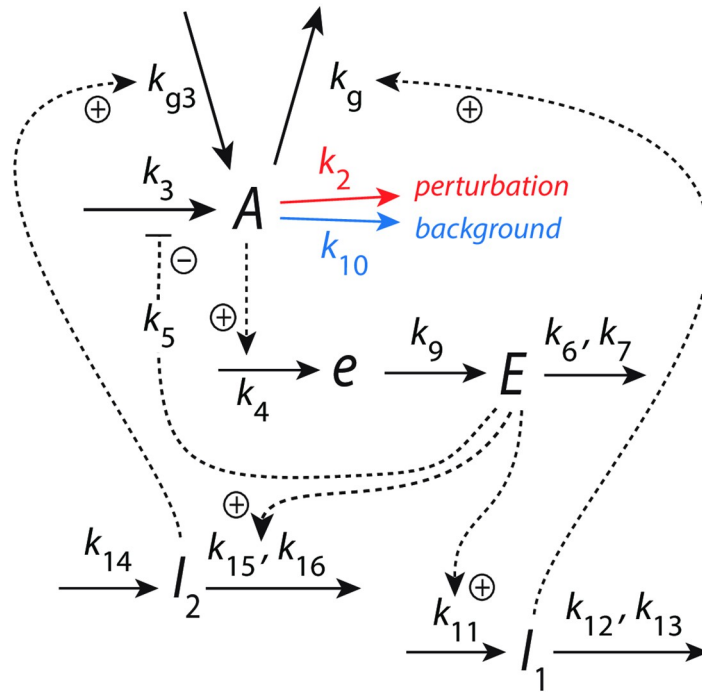


Fig 12. Same scheme as Fig 4a, but to facilitate a non-oscillatory homeostat all A-removing reactions are changed to first-order kinetics with respect to A.

<https://doi.org/10.1371/journal.pone.0287083.g012>

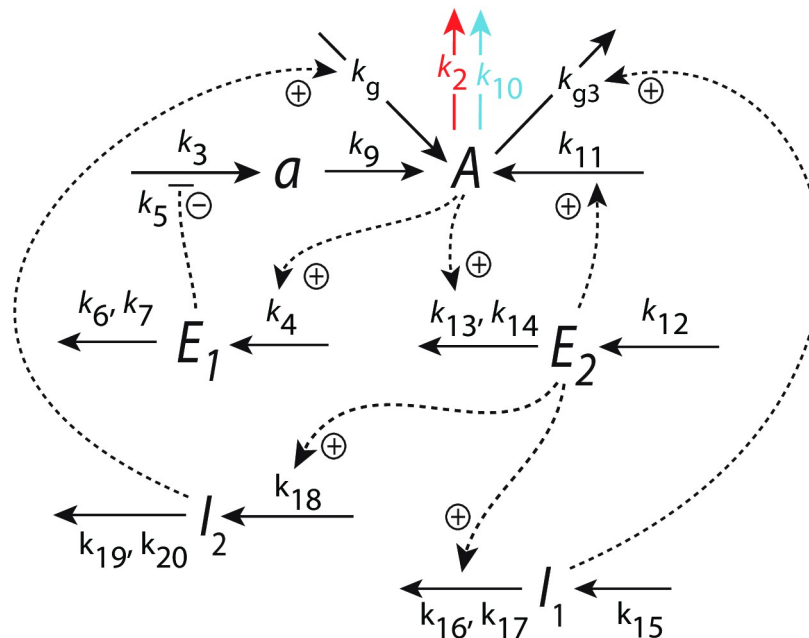


Fig 13. Coherent feedback loop $A-E_2-(I_1, I_2)-A$ with an additional inflow control of A by E_1 . Compound a is a precursor to A, which has been found to promote limit-cycle oscillations, once the system is fully oscillatory [11]. Stepwise perturbations in k_2 (outlined in red) are applied at constant backgrounds levels k_{10} (outlined in blue).

<https://doi.org/10.1371/journal.pone.0287083.g013>

$$\dot{I}_2 = k_{18} \cdot E_2 - \frac{k_{19} \cdot I_2}{k_{20} + I_2} \tag{24}$$

E_1 and E_2 provide two set-points for A : one, $A_{set}^{E_1}$, by setting Eq 21 to zero and solving for the steady state level of A under zero-order conditions, and the other, $A_{set}^{E_2}$, by doing the same for Eq 22. This gives:

$$A_{set}^{E_1} = \frac{k_6}{k_4} \quad (k_7 \ll E_1) \tag{25}$$

and

$$A_{set}^{E_2} = \frac{k_{12}}{k_{13}} \quad (k_{14} \ll E_2) \tag{26}$$

In the calculations we have set $A_{set}^{E_1} = 2.1$ and $A_{set}^{E_2} = 2.0$. Since the E_2 inflow controller has a lower set-point in comparison with E_1 , E_2 will take over the control of A [22], while E_1 will be inactive and allow a constant inflow to A via a .

Fig 14 shows that in this system a $1 \rightarrow 10$ perturbation in k_2 induces a train of damped oscillations with background (k_{10}) independent concentration profiles. In panels a and b ΔA (for definition see inset in Fig 11) is shown as a function of increasing k_2 steps at different but constant k_{10} backgrounds. Panel c shows the time profile in A for a $1 \rightarrow 10$ k_2 step with a k_{10} background of 0. In panel d the same step is applied but now with a background of $k_{10} = 1024$. One clearly sees the conserved background-independent transition profiles in A .

Frequency homeostasis without background compensation. Fig 15a shows an oscillator scheme which we previously described in relation to robust frequency homeostasis [11]. We wondered whether frequency homeostasis without coherent feedback would also lead to background compensation, but realized that this is not the case. In Fig 15a I_1 , I_2 , and E do not feed back coherently to A , but (incoherently) to a , which is a precursor of A .

The rate equations are ('pert' stands for perturbation and 'bg' for background):

$$\dot{A} = k_9 \cdot a - \underbrace{k_2 \cdot A}_{\text{pert}} - \underbrace{k_{10} \cdot A}_{\text{bg}} \tag{27}$$

$$\dot{a} = \left(\frac{k_{g3} \cdot I_2 + k_3}{k_5 + E} \right) \cdot k_5 - k_g \cdot a \cdot I_1 - k_9 \cdot a \tag{28}$$

$$\dot{E} = k_4 \cdot A - \frac{k_6 \cdot E}{k_7 + E} \tag{29}$$

$$\dot{I}_1 = k_{11} \cdot E - \frac{k_{12} \cdot I_1}{k_{13} + I_1} \tag{30}$$

$$\dot{I}_2 = k_{14} - \left(\frac{k_{15} \cdot I_2}{k_{16} + I_2} \right) \cdot E \tag{31}$$

Fig 16 shows an example of oscillations for the scheme in Fig 15 with background $k_{10} = 0$ and a step perturbation in k_2 from 1 (phase 1) to 10 (phase 2). It may be noted that in this case oscillations occur although the removal reactions of a and A are first-order with respect to a

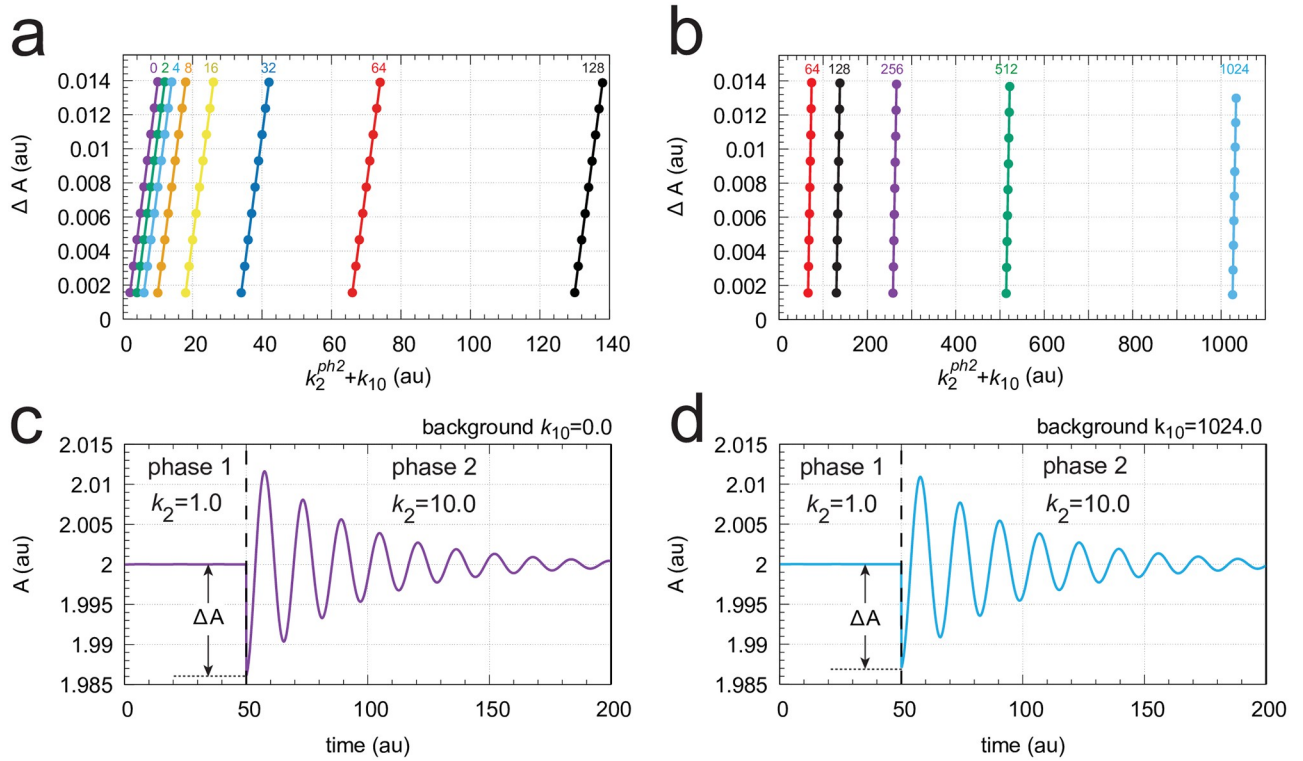


Fig 14. Background compensation by coherent feedback in the scheme of Fig 13. Panels a and b: ΔA as a function of $k_2^{ph2} + k_{10}$ for different but constant backgrounds. k_2^{ph2} is the k_2 value in phase 2. The background values (k_{10}) are indicated above the colored curves. Panels c and d: Concentration profiles in A when a $k_2 \rightarrow 10$ step is applied at respective backgrounds of $k_{10} = 0.0$ and 1024.0 . Other rate constants: $k_3 = 2.5 \times 10^3$, $k_4 = 1.0$, $k_5 = 0.1$, $k_6 = 2.1$, $k_7 = 1 \times 10^{-5}$, $k_9 = 0.5$, $k_{11} = 0.5$, $k_{12} = 200.0$, $k_{13} = 100$, $k_{14} = k_{17} = k_{20} = 1 \times 10^{-5}$, $k_{15} = 1 \times 10^3$, $k_{16} = 10.0$, $k_{18} = 1.0$, $k_{19} = 99.99$, $k_g = k_{g3} = 0.1$. Initial concentrations for c: $A_0 = 2.0$, $E_{1,0} = 2.0 \times 10^{-4}$, $E_{2,0} = 100.0$, $a_0 = 4.99 \times 10^3$, $I_{1,0} = 2.5684 \times 10^3$, $I_{2,0} = 2.8492 \times 10^4$. Initial concentrations for d: $A_0 = 2.0$, $E_{1,0} = 2.0 \times 10^{-4}$, $E_{2,0} = 100.0$, $a_0 = 4.99 \times 10^3$, $I_{1,0} = 3.5195 \times 10^3$, $I_{2,0} = 2.0888 \times 10^3$. Supporting information S1 Data includes the python scripts showing the results of panels c and d.

<https://doi.org/10.1371/journal.pone.0287083.g014>

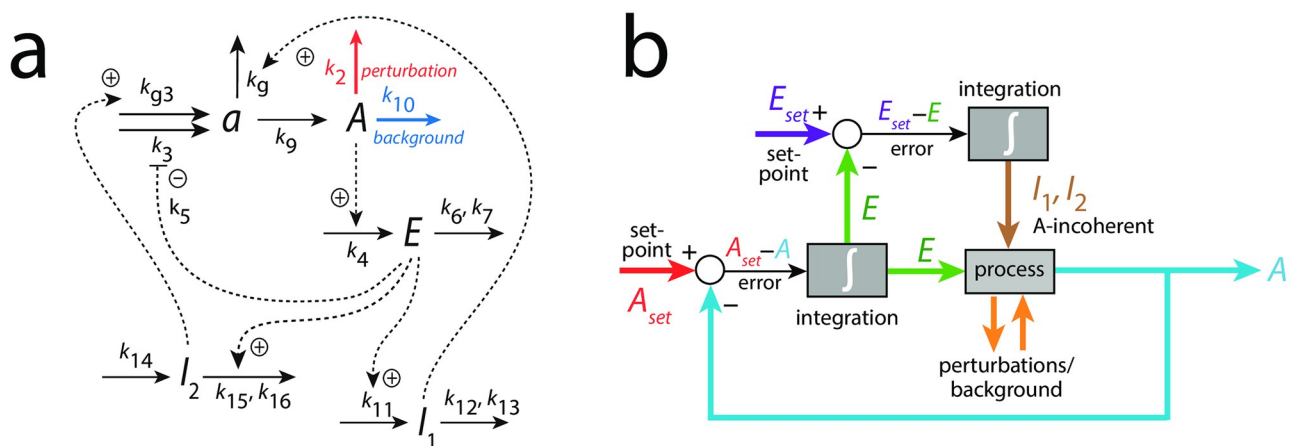


Fig 15. Oscillator based on motif 2 [11, 22] with A -incoherent feedback, where E , I_1 , and I_2 feed back to a , a precursor of A . Panel a: reaction scheme. Panel b: Flow scheme. For rate equations, see main text.

<https://doi.org/10.1371/journal.pone.0287083.g015>

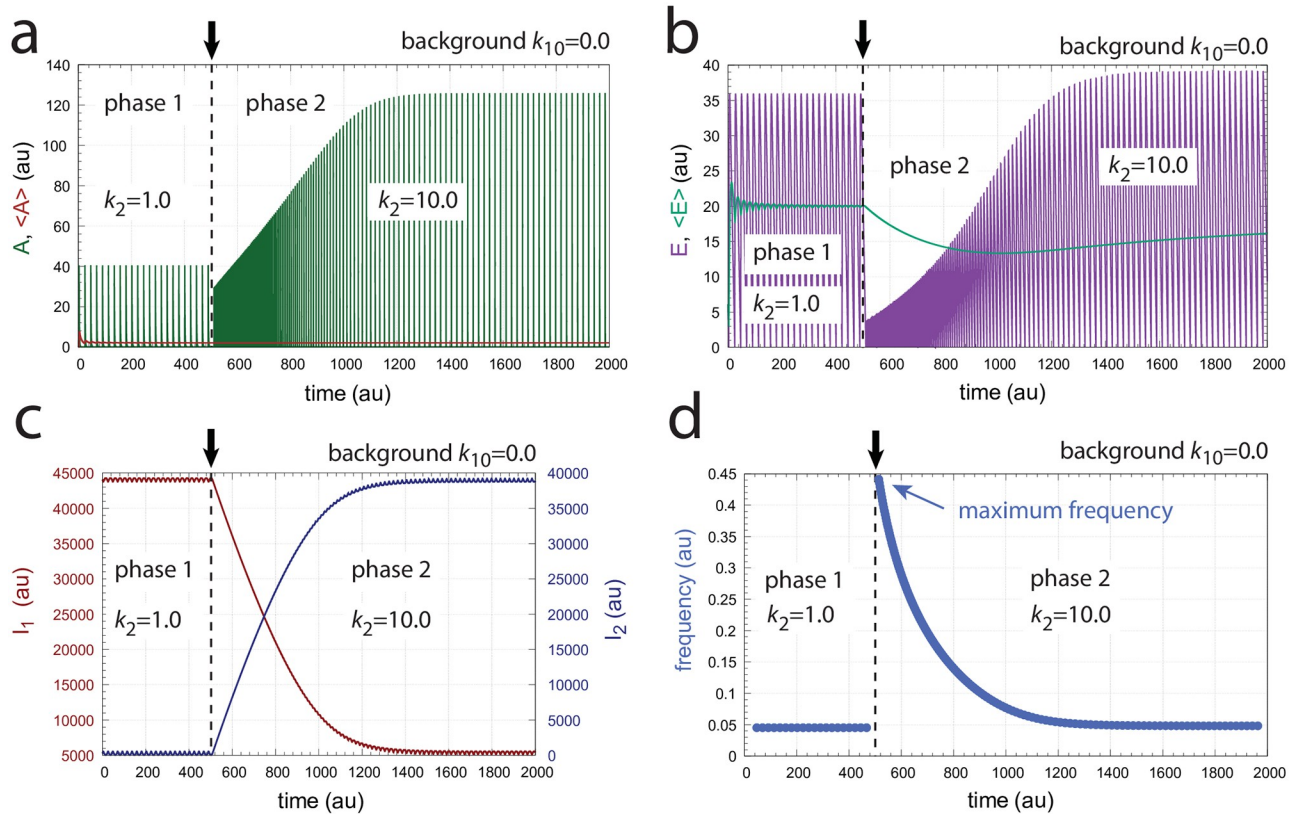


Fig 16. Frequency homeostasis in the oscillator of Fig 15. Background $k_{10} = 0.0$. A k_2 step $1 \rightarrow 10$ occurs at time $t = 500$ indicated by the vertical arrows. Panel a: Concentration of A and average $\langle A \rangle$ as a function of time. Panel b: Concentration of E and average $\langle E \rangle$ as a function of time. Panel c: Concentrations of I_1 and I_2 as a function of time. Panel d: Frequency as a function of time. Other rate constants: $k_3 = 1 \times 10^6$, $k_4 = 1.0$, $k_5 = 1 \times 10^{-6}$, $k_6 = 2.0$, $k_7 = k_{13} = k_{16} = 1 \times 10^{-6}$, $k_9 = 2.0$, $k_{11} = 5.0$, $k_{12} = 100.0$, $k_{14} = 99.99$, $k_{15} = 5.0$, $k_g = 1 \times 10^{-3}$, and $k_{g^3} = 100.0$. Initial concentrations: $A_0 = 5.6920 \times 10^{-3}$, $E_0 = 6.1163$, $a_0 = 3.6221 \times 10^{-3}$, $I_{1,0} = 4.4051 \times 10^4$, $I_{2,0} = 2.7566 \times 10^2$. See S1 Data for python scripts.

<https://doi.org/10.1371/journal.pone.0287083.g016>

and A , indicating that first-order processes are only a ‘weak’ condition to abolish oscillatory behavior, as has been indicated in the above section ‘Background compensation in non-oscillatory homeostats’.

Fig 16 clearly shows the occurrence of frequency homeostasis. However, when the oscillator is tested for different but constant k_{10} backgrounds with changed k_2 steps the maximum frequency decreases with increasing backgrounds. Fig 17a shows the decrease of the maximum frequency and loss of robust background compensation at four different k_{10} backgrounds when k_2 steps are applied from $1 \rightarrow 2$ up to $1 \rightarrow 10$. When using a logarithmic ordinate (Fig 17b) lines appear more or less parallel, which may give the illusion that the system responds in a background compensated way.

Is retinal light adaptation background compensated?

Based on the comment in Ref [2] that the parallel lines in Fig 2 indicate the same response at different backgrounds and involve a form of compensation mechanism, we became interested to look into the conditions how background compensation could occur. This requires of course how the term ‘background compensation’ is defined. In our definition, background compensation implies the presence of a compensatory mechanism, which enables the same

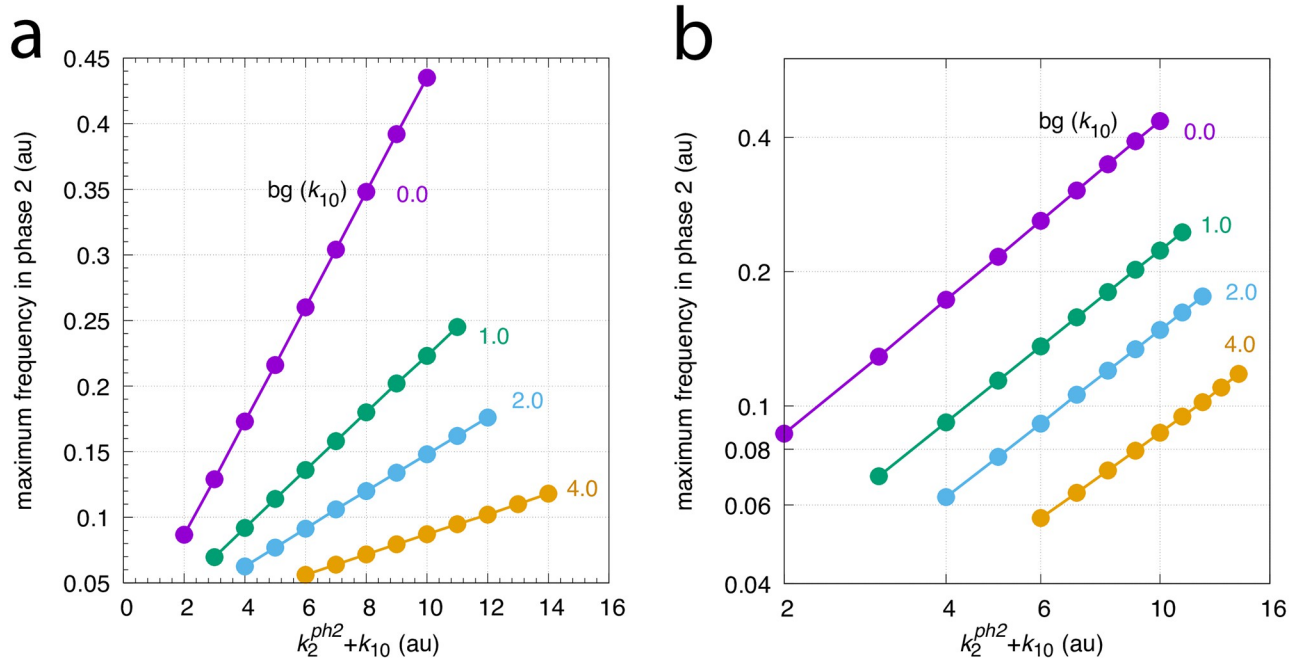


Fig 17. Maximum frequencies as a function of $k_2^{ph2} + k_{10}$, where k_2^{ph2} is the k_2 value in phase 2. Calculations were performed with rate constants as described in Fig 16. Panel a show results with linear scaling of axes, while panel b shows the same data set as double-logarithmic plots. Initial concentrations: $bg(k_{10}) = 0.0$: see legend of Fig 16; $bg(k_{10}) = 1.0$: $A_0 = 2.5946 \times 10^{-3}$, $E_0 = 25.4830$, $a_0 = 2.6844 \times 10^{-3}$, $I_{1,0} = 3.0980 \times 10^4$, $I_{2,0} = 1.3296 \times 10^4$; $bg(k_{10}) = 2.0$: $A_0 = 5.0041 \times 10^{-3}$, $E_0 = 15.8930$, $a_0 = 7.8102 \times 10^{-3}$, $I_{1,0} = 2.2995 \times 10^4$, $I_{2,0} = 2.1181 \times 10^4$; $bg(k_{10}) = 4.0$: $A_0 = 4.7328 \times 10^{-3}$, $E_0 = 21.6050$, $a_0 = 1.2043 \times 10^{-2}$, $I_{1,0} = 1.3516 \times 10^4$, $I_{2,0} = 3.0610 \times 10^4$.

<https://doi.org/10.1371/journal.pone.0287083.g017>

response of a controlled system, *independent* of different but constant backgrounds, which are applied in parallel to a perturbation. The result shown in Fig 2, however, does not meet this definition. As indicated by the vertical dashed bar in the figure, an increase of the background from the red to the blue curve, and from the blue to the green curve, a reduction in the average maximum frequency is observed when a test spot luminance of 9×10^{-2} cd/m² is applied. In fact, the adaptation behavior shown in Fig 1 can show an analogous behavior as in Fig 2.

To see this we use a model described by Dowling [3], where the response amplitude V of retinal cells with respect to a light perturbation I is given by the Hill equation [35]

$$V = \frac{V_{max} I^\alpha}{I^\alpha + \sigma^\alpha} \tag{32}$$

The cooperativity α is 1.0 for photoreceptor cells (changing the Hill equation into a Michaelis-Menten equation), but found to be 0.7 to 0.8 for horizontal cells, 1.2–1.4 for bipolar and sustained ganglion cells, and about 3.4 for transient ganglion cells (for an overview see [3]).

We consider here the response kinetics of rods and cones, i.e. $\alpha = 1$ with

$$V = \frac{V_{max} I}{I + \sigma} \tag{33}$$

As pointed out by Naka and Rushton [36], in the presence of a background I_0 the response V_1 upon a perturbation I_1 of a single pigment system will follow Eq 33, but with an increase of σ to $\sigma_1 = \sigma + I_0$ and a scaling of V_{max} by a factor of $\sigma/(\sigma + I_0)$. This can be shown as follows:

In the presence of a constant background I_0 Eq 33 gives

$$V_0 = \frac{V_{max} I_0}{I_0 + \sigma} \quad (34)$$

If a light perturbation I_1 is applied in addition to background I_0 the total response amplitude is

$$V_1 + V_0 = \frac{V_{max}(I_0 + I_1)}{I_0 + I_1 + \sigma} \quad (35)$$

Subtracting Eq 34 from Eq 35 gives

$$\begin{aligned} V_1 &= V_{max} \left[\frac{(I_0 + I_1)}{I_0 + I_1 + \sigma} - \frac{I_0}{I_0 + \sigma} \right] = V_{max} \left[\frac{(I_0 + I_1) \cdot (I_0 + \sigma) - I_0 \cdot (I_0 + I_1 + \sigma)}{(I_0 + I_1 + \sigma) \cdot (I_0 + \sigma)} \right] \\ &= V_{max} \left[\frac{I_1 \cdot \sigma}{(I_0 + I_1 + \sigma) \cdot (I_0 + \sigma)} \right] = \frac{V_{max} \cdot \sigma}{I_0 + \sigma} \left(\frac{I_1}{I_0 + I_1 + \sigma} \right) \\ &= V_{max,1} \left(\frac{I_1}{I_1 + \sigma_1} \right) \end{aligned} \quad (36)$$

Fig 18 shows Eq 33 with six different σ values which mimic six different background levels. For the sake of simplicity we have set $V_{max} = 1$. In panel a both axes are linear, while in panel b the ordinate is logarithmic and the abscissa is linear. In panel c the ordinate is linear and the abscissa is logarithmic. Finally, in panel d both axes are logarithmic.

Fig 18c is analogous to the results in Fig 2 when for a given perturbation (indicated by the vertical dashed lines) an increased background or an increased σ leads to a reduction in the averaged maximum frequency. No background compensation, as indicated by Kandel et al. in Ref [2] appears necessary.

When studying the photoadaptation of gecko photoreceptors, Kleinschmidt and Dowling [37] showed log-log relationships analogous to Fig 18d. Dowling interpreted the parallel lines as a result of a second adaptive mechanism in the receptor, which shifts the photoreceptor intensity-response curves along the intensity axis, thus extending the range over which the receptor responds (see page 222 in Ref [3], bottom section).

Clearly, as Fig 18 shows, the parallel lines in panels c or d neither require the need for a background compensation mechanism nor additional adaptive mechanisms. While adaptation mechanisms compensating for a background cannot be excluded, the observation of parallel lines in semi-logarithmic or double-logarithmic plots appear not sufficient to indicate additional background compensation mechanisms besides of the negative feedbacks which lead to the responses in Fig 1 [5].

Conclusion and outlook

We have shown how robust background compensation in oscillatory and non-oscillatory homeostatic controllers can be realized. The needed feedback condition has been termed ‘coherent feedback’ in analogy to a corresponding concept applied in quantum control theory. Although the property of robust background compensation appears interesting, we are presently not aware of any biological or biochemical example that shows or applies this property. Background compensation may become of interest in synthetic biology to design cellular responses, which by some reason are needed to become background independent. Concerning the case of retinal light adaptation, parallel lines in semi-logarithmic or double-logarithmic

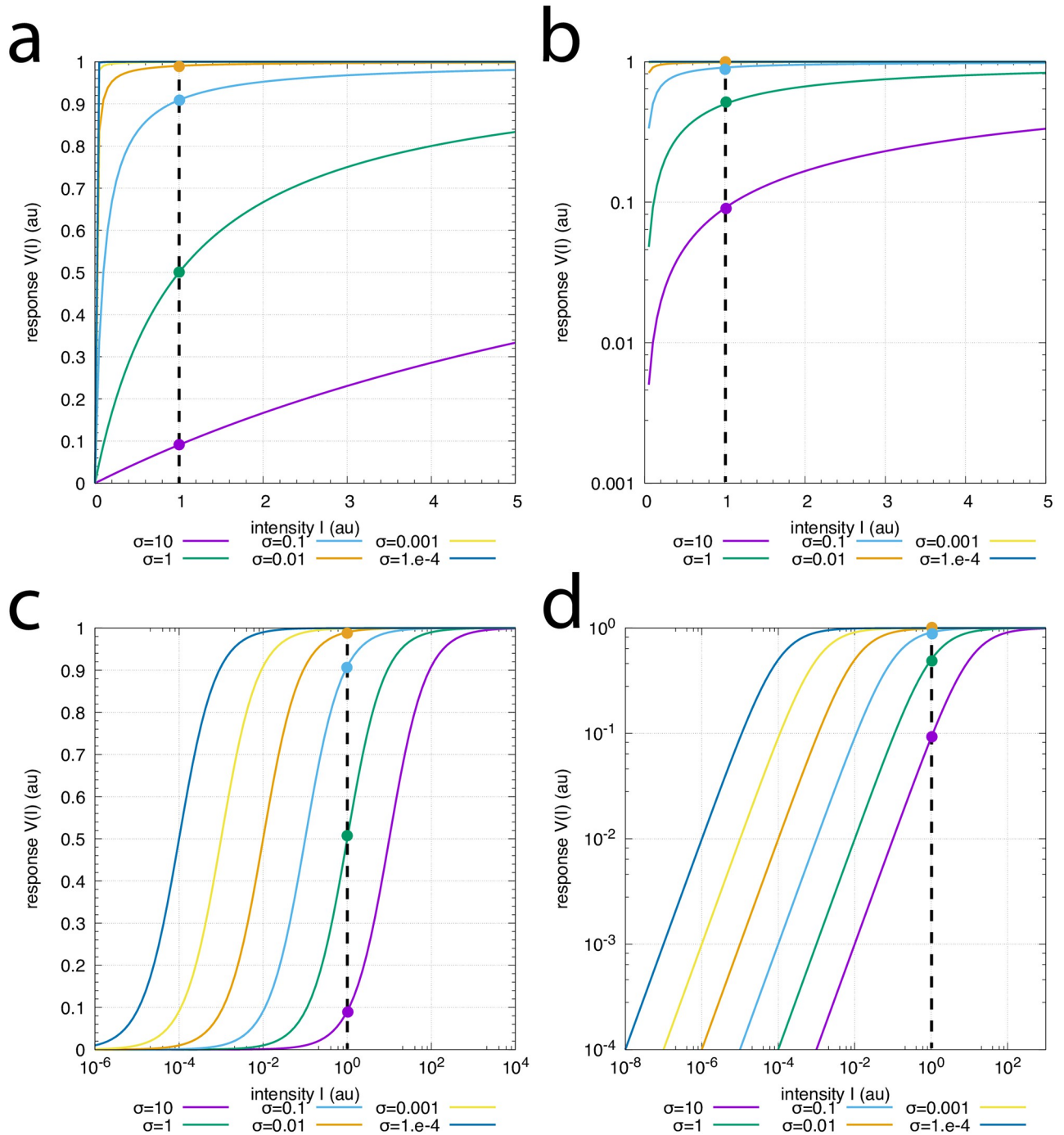


Fig 18. Photoadaptation behaviors in rods and cones described by the Michaelis-Menten equation (Eq 33). The colored lines in the panels show Eq 33 with σ values ranging over six orders of magnitudes from $\sigma = 1 \times 10^{-4}$ up to $\sigma = 10$. For simplicity, $V_{max} = 1$. Panel a: Both axes are linear. Panel b: Ordinate is logarithmic and abscissa is linear. Panel c: Ordinate is linear and abscissa is logarithmic. Panel d: Both axes are logarithmic. The dashed vertical lines indicate a perturbation intensity of $I = 1$. The colored intersection points with the vertical dashed lines show the responses of V for the different backgrounds with the same color.

<https://doi.org/10.1371/journal.pone.0287083.g018>

plots do not necessarily imply the presence of background compensating mechanisms as defined in this paper.

Supporting information

S1 Data. Documentation. A zip-file with python scripts describing the results for Figs 5, 6, 9a, 9b, 12b, 12c, 14c, 14d, and 16.
(ZIP)

Author Contributions

Conceptualization: Peter Ruoff.

Formal analysis: Melissa Nygård, Peter Ruoff.

Investigation: Melissa Nygård, Peter Ruoff.

Software: Melissa Nygård, Peter Ruoff.

Validation: Peter Ruoff.

Visualization: Melissa Nygård.

Writing – original draft: Peter Ruoff.

Writing – review & editing: Melissa Nygård, Peter Ruoff.

References

1. Clancy J, McVicar AJ. *Physiology and Anatomy. A Homeostatic Approach*. Hodder Arnold; 2002.
2. Kandel ER, Koester JD, Mack SH, Siegelbaum S, editors. *Principles of Neural Science*. Sixth Edition. McGraw-Hill; 2021.
3. Dowling JE. *The Retina: An Approachable Part of the Brain*. Revised Edition. Harvard University Press; 2012.
4. Purves D, Augustine GJ, Fitzpatrick D, Hall WC, LaMantia AS, McNamara JO, et al. *Neuroscience*. Fourth Edition. Sinauer Associates, Inc.; 2008.
5. Grini JV, Nygård M, Ruoff P. Homeostasis at different backgrounds: The roles of overlaid feedback structures in vertebrate photoadaptation. *PLoS One*. 2023; 18(4):e0281490. <https://doi.org/10.1371/journal.pone.0281490> PMID: 37115760
6. Fain GL, Matthews HR, Cornwall MC, Koutalos Y. Adaptation in vertebrate photoreceptors. *Physiological Reviews*. 2001; 81(1):117–151. <https://doi.org/10.1152/physrev.2001.81.1.117> PMID: 11152756
7. Schneeweis D, Schnapf J. Noise and light adaptation in rods of the macaque monkey. *Visual Neuroscience*. 2000; 17(5):659–666. <https://doi.org/10.1017/S0952523800175017> PMID: 11153647
8. Sakmann B, Creutzfeldt OD. Scotopic and mesopic light adaptation in the cat's retina. *Pflügers Archiv*. 1969; 313:168–185. PMID: 5390975
9. Lloyd S. Coherent quantum feedback. *Physical Review A*. 2000; 62(2):022108. <https://doi.org/10.1103/PhysRevA.62.022108>
10. Fan B, Ning J, Xie M, Liu C, Guan S. Coherent feedback induced transparency. *Optics Express*. 2020; 28(19):28243–28251. <https://doi.org/10.1364/OE.404053> PMID: 32988100
11. Thorsen K, Agafonov O, Selstø CH, Jolma IW, Ni XY, Drengstig T, et al. Robust concentration and frequency control in oscillatory homeostats. *PLoS One*. 2014; 9(9):e107766. <https://doi.org/10.1371/journal.pone.0107766> PMID: 25238410
12. Radhakrishnan K, Hindmarsh AC. Description and Use of LSODE, the Livermore Solver for Ordinary Differential Equations. NASA Reference Publication 1327, Lawrence Livermore National Laboratory Report UCRL-ID-113855. Cleveland, OH 44135-3191: National Aeronautics and Space Administration, Lewis Research Center; 1993.
13. Lewis FL. *Applied Optimal Control & Estimation*. Englewood Cliffs, NJ: Prentice Hall; 1992.
14. Bennett S. A brief history of automatic control. *IEEE Control Systems Magazine*. 1996; 16(3):17–25. <https://doi.org/10.1109/37.506394>

15. Warwick K. An Introduction to Control Systems. Second Edition. World Scientific; 1996.
16. Wilkie J, Johnson M, Reza K. Control Engineering. An Introductory Course. New York: Palgrave; 2002.
17. Yi TM, Huang Y, Simon MI, Doyle J. Robust perfect adaptation in bacterial chemotaxis through integral feedback control. PNAS. 2000; 97(9):4649–4653. <https://doi.org/10.1073/pnas.97.9.4649> PMID: 10781070
18. Iglesias PA, Ingalls BP. Control Theory and Systems Biology. MIT Press; 2010.
19. Ang J, Bagh S, Ingalls B, McMillen D. Considerations for using integral feedback control to construct a perfectly adapting synthetic gene network. J Theor Biol. 2010; 266(4):723–738. <https://doi.org/10.1016/j.jtbi.2010.07.034> PMID: 20688080
20. Del Vecchio D, Dy AJ, Qian Y. Control theory meets synthetic biology. Journal of The Royal Society Interface. 2016; 13(120):20160380. <https://doi.org/10.1098/rsif.2016.0380> PMID: 27440256
21. Aoki SK, Lillacci G, Gupta A, Baumschlager A, Schweingruber D, Khammash M. A universal biomolecular integral feedback controller for robust perfect adaptation. Nature. 2019; 570(7762):533–537. <https://doi.org/10.1038/s41586-019-1321-1> PMID: 31217585
22. Drengstig T, Jolma I, Ni X, Thorsen K, Xu X, Ruoff P. A basic set of homeostatic controller motifs. Biophys J. 2012; 103(9):2000–2010. <https://doi.org/10.1016/j.bpj.2012.09.033> PMID: 23199928
23. Ni XY, Drengstig T, Ruoff P. The control of the controller: Molecular mechanisms for robust perfect adaptation and temperature compensation. Biophys J. 2009; 97:1244–53. <https://doi.org/10.1016/j.bpj.2009.06.030> PMID: 19720012
24. Ang J, McMillen D. Physical constraints on biological integral control design for homeostasis and sensory adaptation. Biophys J. 2013; 104(2):505–15. <https://doi.org/10.1016/j.bpj.2012.12.015> PMID: 23442873
25. Briat C, Gupta A, Khammash M. Antithetic integral feedback ensures robust perfect adaptation in noisy biomolecular networks. Cell Systems. 2016; 2(1):15–26. <https://doi.org/10.1016/j.cels.2016.01.004> PMID: 27136686
26. Waheed Q, Zhou H, Ruoff P. Kinetics and mechanisms of catalyzed dual-E (antithetic) controllers. PLoS One. 2022; 17(8):e0262371. <https://doi.org/10.1371/journal.pone.0262371> PMID: 35980978
27. Shoval O, Goentoro L, Hart Y, Mayo A, Sontag E, Alon U. Fold-change detection and scalar symmetry of sensory input fields. PNAS. 2010; p. 201002352. <https://doi.org/10.1073/pnas.1002352107> PMID: 20729472
28. Drengstig T, Ni XY, Thorsen K, Jolma IW, Ruoff P. Robust adaptation and homeostasis by autocatalysis. J Phys Chem B. 2012; 116:5355–5363. <https://doi.org/10.1021/jp3004568> PMID: 22506960
29. Briat C, Zechner C, Khammash M. Design of a synthetic integral feedback circuit: dynamic analysis and DNA implementation. ACS Synthetic Biology. 2016; 5(10):1108–1116. <https://doi.org/10.1021/acssynbio.6b00014> PMID: 27345033
30. Fjeld G, Thorsen K, Drengstig T, Ruoff P. Performance of homeostatic controller motifs dealing with perturbations of rapid growth and depletion. J Phys Chem B. 2017; 121(25):6097–6107. <https://doi.org/10.1021/acs.jpcc.7b01989> PMID: 28571313
31. Nishiyama N, Ruoff P, Jimenez JC, Miwakeichi F, Nishiyama Y, Yata T. Modeling the interaction between donor-derived regulatory T cells and effector T cells early after allogeneic hematopoietic stem cell transplantation. Biosystems. 2023; 227–228:104889. <https://doi.org/10.1016/j.biosystems.2023.104889> PMID: 37019377
32. Bhattacharya P, Raman K, Tangirala AK. Discovering adaptation-capable biological network structures using control-theoretic approaches. PLOS Computational Biology. 2022; 18(1):e1009769. <https://doi.org/10.1371/journal.pcbi.1009769> PMID: 35061660
33. Bhattacharya P, Raman K, Tangirala AK. On biological networks capable of robust adaptation in the presence of uncertainties: A linear systems-theoretic approach. Mathematical Biosciences. 2023; 358:108984. <https://doi.org/10.1016/j.mbs.2023.108984> PMID: 36804384
34. Ponsiglione AM, Montefusco F, Donisi L, Tedesco A, Cosentino C, Merola A, et al. A General Approach for the Modelling of Negative Feedback Physiological Control Systems. Bioengineering. 2023; 10(7):835. <https://doi.org/10.3390/bioengineering10070835> PMID: 37508862
35. Segel IH. Enzyme Kinetics: Behavior and Analysis of Rapid Equilibrium and Steady State Enzyme Systems. Wiley; 1975.
36. Naka KI, Rushton WA. S-potentials from luminosity units in the retina of fish (Cyprinidae). The Journal of Physiology. 1966; 185(3):587–599. <https://doi.org/10.1113/jphysiol.1966.sp008003> PMID: 5918060
37. Kleinschmidt J, Dowling JE. Intracellular recordings from Gecko photoreceptors during light and dark adaptation. The Journal of General Physiology. 1975; 66(5):617–648. <https://doi.org/10.1085/jgp.66.5.617> PMID: 1194887